Article

Dual-Polarized Dipole Antenna with Wideband Stable Radiation Patterns Using AMC Reflector

Xianjing Lin , Jielin Mai , Hong Jun He , Yao Zhang [*]

Article

Dual-Polarized Dipole Antenna with Wideband Stable Radiation Patterns Using AMC Reflector

Xianjing Lin [1], Jie Lin Mai [1], Hong Jun He[1], Yao Zhang [2]*

[1] School of Electronic Engineering and Intelligence, Dongguan University of Technology, Dongguan, Guangdong 523808, P.R. China;

[2] Institute of Electromagnetics and Acoustics, Xiamen University, Xiamen, Fujian 361005, China.

* Correspondence: zhangsantu@xmu.edu.cn(Y.Z.)

Abstract: This paper presents a wideband dual-polarized dipole antenna structure operating at 1.7-3.8 GHz (76.4%). For a traditional 4G dipole antenna which covers the band 1.71 GHz- 2.69 GHz, it's difficult to maintain the satisfactory impedance matching and normal stable radiation patterns within the 5G sub-6 GHz band 3.3-3.8 GHz, which mainly due to the fixed antenna height is no longer a quarter-wavelength. To solve this, a connected-ring-shaped metasurface structure is proposed and deployed to operate as an artificial magnetic conductor (AMC). As a result, stable antenna radiation patterns are obtained within the whole band 1.7-3.8 GHz. For verification, this wideband dipole antenna using AMC is implemented and tested. The measured results show that the proposed antenna has an impedance bandwidth of 80.7% (1.7-4.0 GHz). It has an average measured in-band realized gain of 7.0 ± 1.0 dBi and a stable $70° \pm 5°$ half power beam width (HPBW) within the 4G/5G-sub 6GHz bands 1710-2690 MHz and 3300-3800 MHz..

Keywords: Wideband antenna; dual-polarized antenna; dipole antenna; radiation pattern restoration

1. Introduction

Dual-polarized dipole antenna has been widely used in the base-station antenna array scenario as the basic antenna array element [1–5].The antennas operate at 1710-2690 MHz[1], [6–10] and 3300-3800 MHz [11] bands are widely used in sub-6GHz base-station application.The antenna designers are devoted to developing wideband antennas which simultaneously cover the above two frequency bands.

However, it's challenging to maintain stable antenna radiation patterns with a fixed antenna height in such a wide frequency band 1710-3800 MHz. Two mainstream approaches are used to solve this problem. One is to design dual-band or notched band antennas operate at the two target frequency bands 1710-2690 MHz and 3300-3800 MHz [12,13]. The other method is to use parasitic components to increase the impedance bandwidth [14–18]. In [14], an extra pair of shorted dipoles were added, and the impedance bandwidth was increased to 74.5% (1.69-3.7 GHz). In [15],parasitic elements such as metal cylinders and triangle metal palates were involved, and the antenna realized a 78.6% bandwidth (1.59-3.65 GHz). However, for the above two designs, the antenna gains at upper-band frequencies (>3 GHz) decreased/increased a lot, indicating unstable radiation patterns. To improve the radiation performance in upper-band frequencies, the design in [16] printed a circular patch and four pairs of dipole strips on an extra substrate layer. Stable radiation patterns over the entire frequency band were realized. However, since this layer substrate is installed above the antenna structure, it inevitably increases the overall antenna profile, which is undesirably for base station applications. Other components such as parasitic posts [17], partially coupled stubs [18], etc., have also been applied to stabilize the antenna radiation patterns recently. With regard to this problem, this work utilized a connected-ring-shaped metasurface structure as an artificial magnetic conductor (AMC). As a result, a dual-polarized cross-dipole antenna achieved an average in-band realized gain of 7.0 ± 1.0 dBi and a stable $70° \pm 5°$ half power beam width (HPBW) within the band 1.7-3.8 GHz.

2. Wideband Antenna Design

2.1. Problem of Traditional Wideband Antenna

Figure 1.(a) diagrams a traditional directional dipole antenna using a reflector. Suppose this antenna operates at 1.7-3.8 GHz and the antenna height h is set to be quarter wavelength of 2.2 GHz ($\lambda_{2.2}$ GHz), which is the center operating frequency of the band 1.71-2.69 GHz. As is known, the antenna radiation patterns at upper-band frequencies are distorted since the fixed antenna height is no longer quarter-wavelength at thesefrequencies. Fig. 1.(b) illustrates the antenna radiation patterns at 2.2 GHz, 3.0 GHz and 3.8 GHz. As seen, the radiation patterns at 3.0 and 3.8 GHz are not stable or even distorted. This is because the 3 dB beamwidth increases as the frequency enhances from 1.7 GHz to 2.8 GHz. However, it decreases drastically when the frequency is larger than 3.6 GHz.
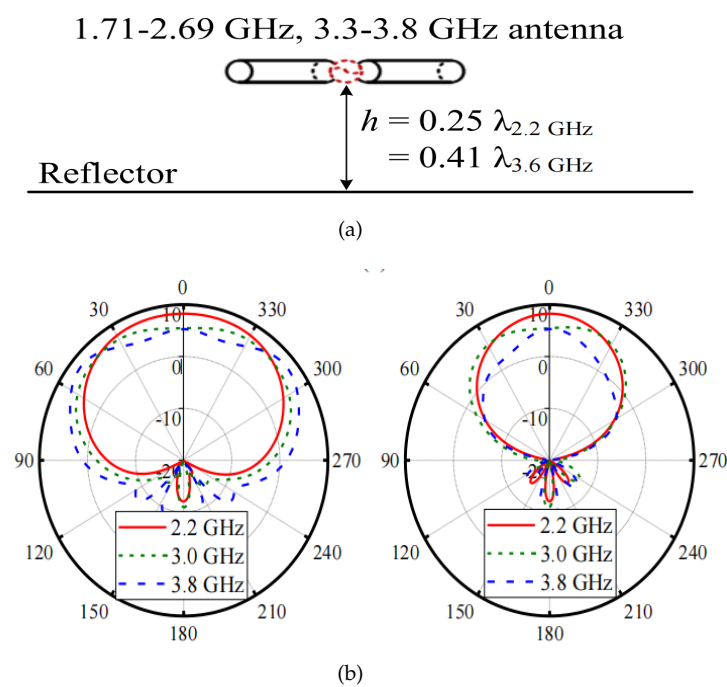

Figure 1. (a) Diagram and (b) H-/E-plane radiation patterns of a 1.7-3.8 GHz antenna.

To solve this problem, this letter proposed a wideband dual-polarized dipole antenna with normal stable radiation patterns within the band 1.7-3.8 GHz, as shown in Figure 2. It consists of three parts: a dipole antenna radiator, a connected-ring-shaped metasurface structure as the AMC and a ground as the reflector. The AMC structure is inserted between the antenna radiator and the reflector and therefore it does not increase the overall antenna height. The antenna radiators are excited by a pair of Y-shaped feedlines which are directly connected to two coaxial cables. The AMC structure is realized by a 7×7 connected ring array. This AMC is deliberately designed to operate at upper-band frequencies (3.3-3.8 GHz) for phase shift compensation. Detailed parameter values are also included in Figure 2. The design procedure and working principle are investigated and revealed in the following part.
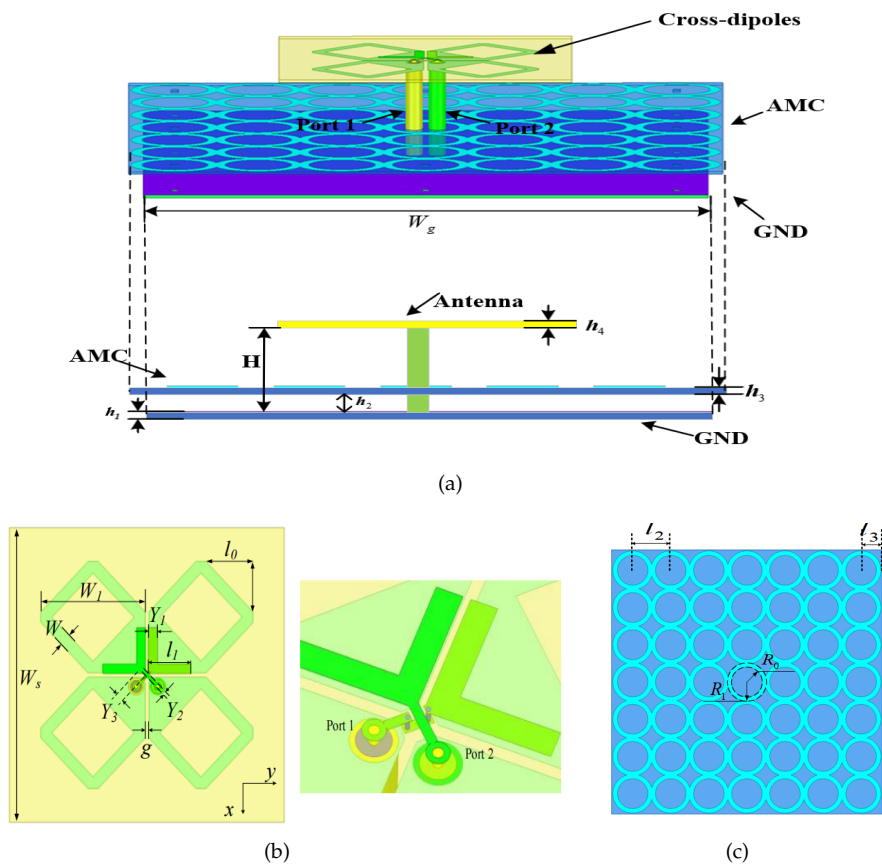
(a)

(b)   (c)

Figure 2. Geometry of the proposed wideband antenna, (a) total view, (b) dipole antenna and (c) AMC (H=30, h_1=1, h_2=2.5,h_3=0.8, h_4=0.8,l_0=12,l_1=10.9, l_2=20,l_3=11,W=1.7, W_s=70, W_g=135,W_1=26.5,Y_1=2.3, Y_2=0.8,Y_3=2.0,g=1, R_1=10.6,R_2=8.1, all in mm).

2.2. Design Procedure

Figure 3 depicts the structures of four reference antennas denoted as Antenna I, II, III, IV. The original Antenna I is a dipole antenna with rectangular radiators and Y-shaped coupled feedlines [7]. To enhance the antenna impedance bandwidth and maintain stable radiation patterns, this structure is then modified to the Antenna II, III, and IV. The simulation results of the four antennas including the reflection coefficient S_{11}, isolation parameter S_{12}, realized gain and HPBW are plotted and compared in Figure 4. As observed, the Antenna I has limited impedance bandwidth (41.2%, 1.64 GHz 2.49 GHz).
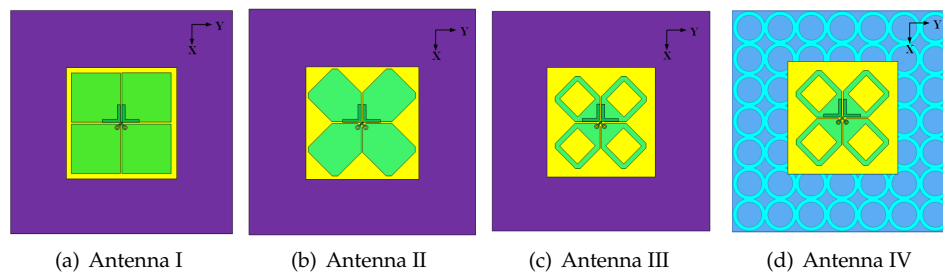

(a) Antenna I   (b) Antenna II   (c) Antenna III   (d) Antenna IV

Figure 3. Structures of the antenna (a) I, (b) II, (c) III and (d) IV.

However, the Antennas II, III, and IV are well matched within the band 1.7-3.8 GHz and the port-to-port isolation $|S_{12}|$ is better than 25 dB. It's noted that the realized gains and HPBW of the four antennas differ a lot, especially at upper-band frequencies (3.0-3.8 GHz). Within the band 1.7-3.8

GHz, the Antenna IV has a stable realized gain ranging from 7.0 dBi to 9.1 dBi. The HPBW is also stable within the range 70°±5°.

2.3. AMC Working Principle

For an antenna, the reflector is an important factor affecting its radiation performance, and analyzing the formation principle of its reflection phase characteristics is the key to study the reflector. Assuming there is an electromagnetic wave that is vertically incident on the reflector, a coordinate system is established based on the material surface, as shown in Figure 5(a). The corresponding equivalent model is shown in Figure 5(b). The transmission line network can be used to calculate the reflection coefficient:

$$\Gamma = \frac{Z_S - Z_0}{Z_S + Z_0} = |\Gamma|e^{\pm i\phi} \tag{1}$$

$$\phi = im\left\{ In\left(\frac{Z_S - Z_0}{Z_S + Z_0}\right)\right\} = im\left\{ In\left(\frac{Z_S - \eta}{Z_S + \eta}\right)\right\} \tag{2}$$

where Z_S is regarded as the impedance of the material surface, Z_0 is the impedance of the dipole antenna, and φ is the phase difference between the incident and the reflected wave of the electromagnetic wave. When $Z_S = 0$,then$\Gamma = 1$,$\phi = \pi$ It can be seen that when the surface impedance is an ideal electrical conductor, the reflection phase of the reflector is 180°. Only when the distance between the radiator and the reflector is $\lambda/4$, the phase difference with a spatial phase delay of 180° can be offset with the 180° phase difference generated by the reflector, so that the reflected wave is in the same direction as the main radiation beam. Thus, enhanced radiation is obtained.
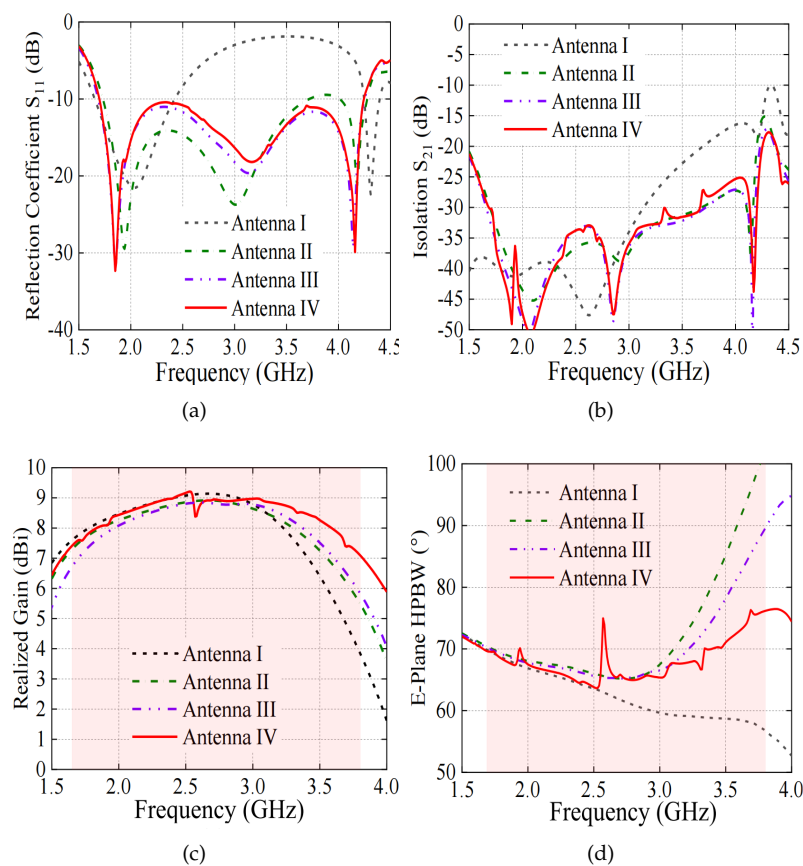

Figure 4. Antenna results including (a) reflection coefficient S_{11}, (b) isolation parameter S_{12}, (c) realized gain and (d) HPBW.
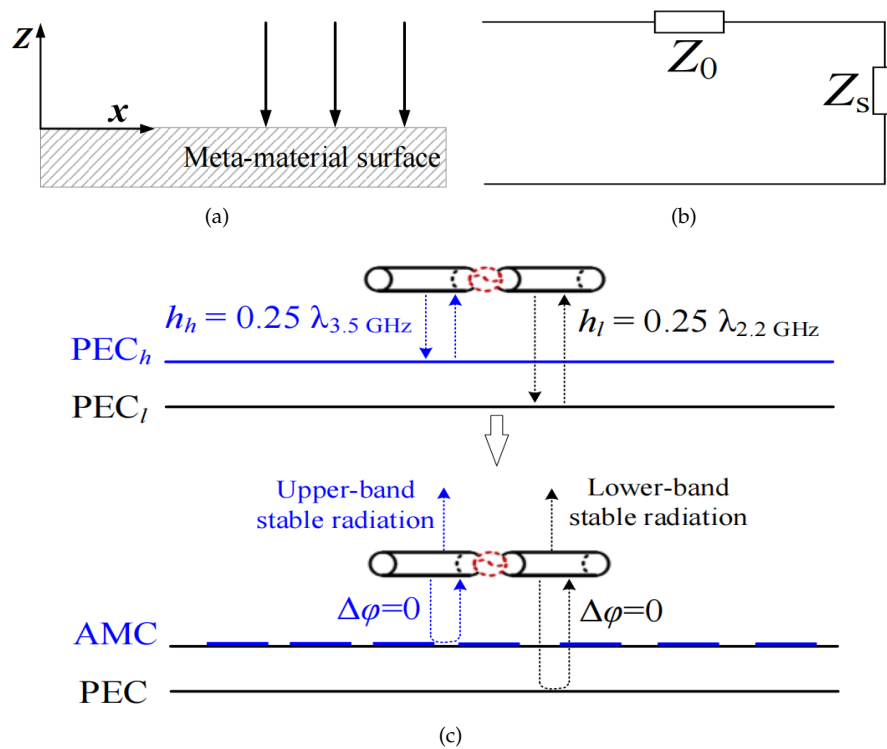
Figure 5. Diagram of the Antenna IV working principle (a) electromagnetic waves incident on the surface of the material, (b) equivalent single port model and (c) constructive interference of the antenna.

According to the above analysis, when the antenna height is set around $\lambda/4$ (λ denotes the wavelength of center frequency 2.2 GHz), the impedance bandwidth for normal stable radiation patterns of a traditional dipole antenna is about 45.4% (1.7-2.7 GHz). To maintain normal stable radiation patterns at 2.7-3.8 GHz, another perfect electric conductor (PEC_h) is required. This PEC_h can be realized by using an AMC, as diagramed in Figure 5(c). The surface impedance of an AMC is very high over a certain frequency region, so it's also known as a high-impedance surface, which is a type of frequency selective surface or meta-material surface.

The schematic diagram and equivalent circuit of the AMC is shown in Figure 6. The AMC reflector consists of a group of AMC units (metal ring patch) arranged periodically. The capacitor is generated between the metal ring patches, and the inductance is generated between the ground plane and the patches, so the AMC structure can be denoted as a series of LC circuits in parallel. According to the circuit principle, the resonant frequency of the AMC can be obtained as:

$$f = \frac{1}{2\pi\sqrt{\frac{C_1 C_2}{C_1 + C_2} L_1}} \tag{3}$$

To search for the frequency band in which the periodic structure behaves as an AMC, a finite element method (FEM) model is established based on the Bloch-Floquet theory [[19]]. A single unit cell of the structure, with periodic boundary conditions (PBC) along its four sides, is simulated as seen in Figure 7(a) to model an infinite periodic surface. The reflected phase from the periodic surface is normalized to the one from the PEC by
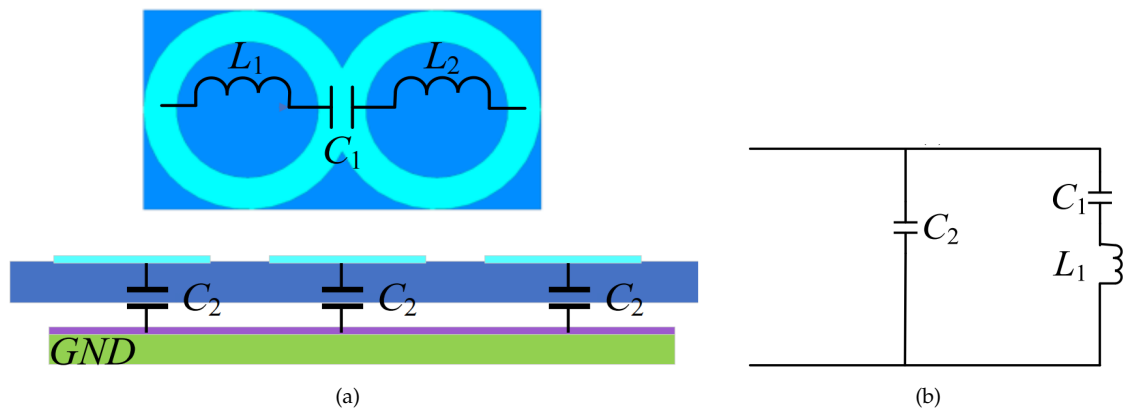
$$\theta = \theta_{FSS} - \theta_{PEC} + \pi \tag{4}$$

Figure 6. (a) Schematic diagram and (b) equivalent circuit of the AMC.
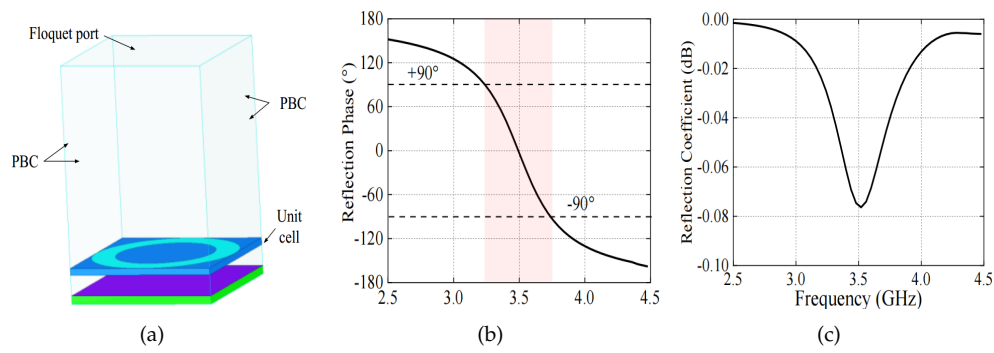

Figure 7. (a) Simulation model and (b) results including the reflection phase and coefficient for determining the reflection properties of the AMC.

The characteristics of the AMC behavior can be verified by calculating the reflection coefficient for a uniform incident plane wave. The phase of the reflection coefficient of an AMC should exhibit a difference of 180° compared to that of a PEC plane. The reflection phase and magnitude of normally incident plane are shown in Figure 7 (b). As observed, the reflection phase on the AMC plane varies continuously from -180° to 180° against frequency and is zero at the resonance frequency. The reflection coefficient is larger than -0.1 dB, indicating almost all the incident waves are reflected. The useful bandwidth of AMC performance is in general defined as +90° to -90° on either side of the resonance frequency. The AMC bandwidth can be obtained as

$$BW_{AMC} = \left[\left(f_{up} - f_{lo} / f_c \right) \right] \times 100\% \tag{5}$$

where f_{up} and f_{lo} are the frequencies at which reflection phase equals -90° and 90°, respectively. f_c is the center frequency where reflection phase equals 0°. The AMC frequency bandwidth of the proposed structure is about 16.6% (3.2-3.78 GHz).

In addition, the operating frequency of the AMC can be shifted to desired values. Figure 8 illustrates the reflection phase of the AMC against the unit cell size AMC_L, unit cell height AMC_H and the ring dimensions. As seen, the center operating frequency as well as the bandwidth can be easily controlled and optimized. Based on such a structure, the radiation patterns of a dipole antenna within the upper frequency band 2.7-3.8 GHz can be restored without increasing the overall antenna height.
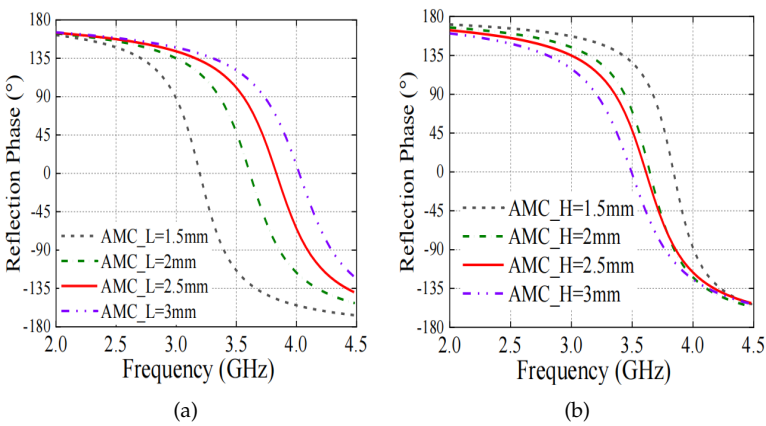
Figure 8. Reflection phase related to different (a) unit cell size AMC_L and (b) unit cell height AMC_H.

3. Dual-Polarized Antenna Implementation

The proposed dual-polarized antenna was designed, fabricated and measured, as shown in Figure 9. The optimization was performed using high frequency structural simulator (HFSS) and the measurement was accomplished by Agilent N5227A network analyzer and Satimo system. Figure 10 shows the results including the S-parameters and radiation response. The simulation results agree well with the measurement ones. As seen, the measured bandwidth ($|s_{11}| < $ -10 dB) is 76.4% (1.7 GHz-3.8 GHz). The measured isolation between two ports within this band is lower than -25 dB and the average measured in-band gain is about 7.5 dBi. A stable 70°±5° half power beam width (HPBW) within the band 1.7-3.8 GHz is obtained. The antenna radiation patterns at 1.7 GHz, 2.7 GHz, 3.3 GHz and 3.8 GHz are plotted in Figure 11 when Port1 is excited. As expected, normal stable radiation patterns with low cross-polarization levels are observed.

Table 1. Comparison Of The Five Wideband Dual-Polarized Antennas.

	Freq.(GHz)	Implementation	HBPW(°)	Realize gain (dBi)
[12]	1.67-2.72 3.3-3.9	Parasitic director + baffle	67.5±8.5 64±5	8.1±0.5 8.35±0.25
[13]	1.71-2.69 3.35-3.6	Notch band antenna	69.5±4 90±10	8.1±0.4 6.6±0.5
[16]	1.7-5.1	Parasitic elements on superstrate	65±5	8.2±0.7
[18]	1.68-3.94	Parasitic strips and posts	66±8	7.5±0.7
This work	**1.7-3.8**	**AMC**	**70±5**	**7.0±1.0**

To address the advantages of the proposed work, the comparison results with other related designs are tabulated in Table1. Dual-band or notched band antenna concept was adopted in [12]-[13] and stable radiation patterns were obtained within the target bands 1.71-2.69 GHz and 3.3-3.8 GHz. In [16], an extra superstrate was deployed to print parasitic elements and thus the antenna overall height was increased. Also, parasitic strips and posts were applied in [18] to achieve a stable realized gain curve. Different from the abovementioned methods, by inserting an AMC structure between the antenna radiator and ground, wideband operation and normal stable radiation patterns were realized in the proposed work.

(a)   (b)
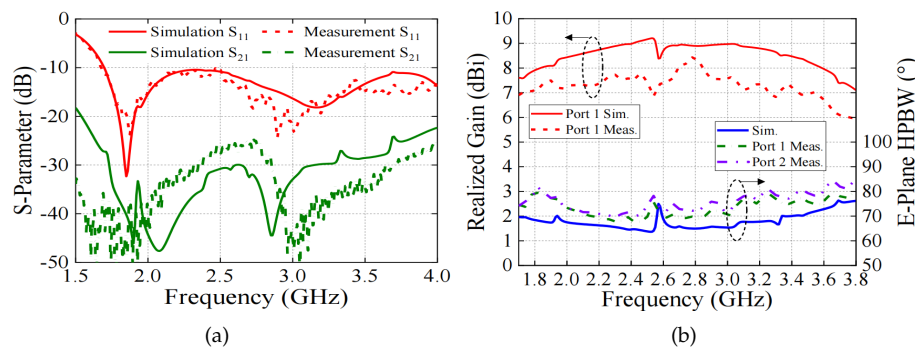
Figure 9. Antenna fabrication prototype.

(a)   (b)

Figure 10. Simulation and measurement results including (a) S-parameters and (b) realized gains, HPBW.

(a)   (b)   (c)   (d)

(e)   (f)   (g)   (h)
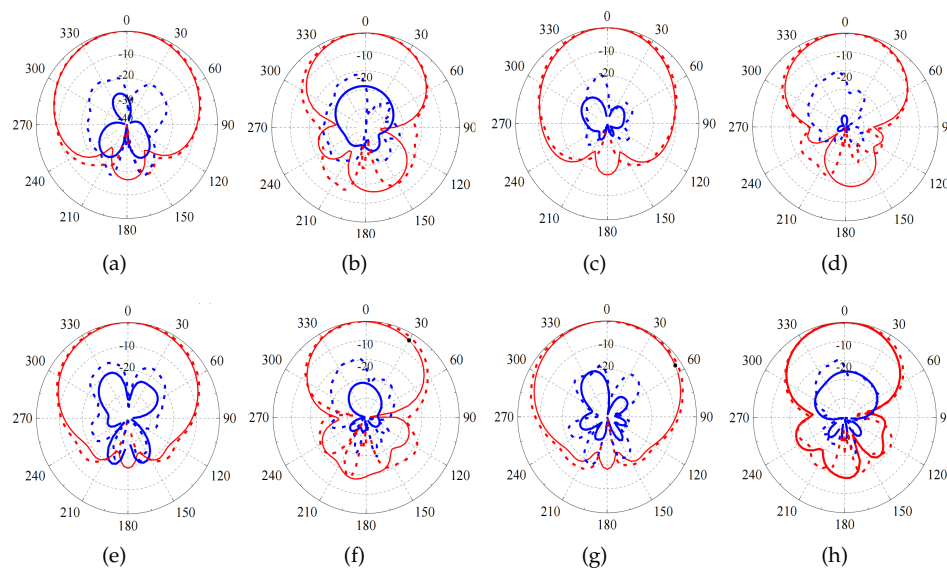
Figure 11. Simulation and measurement radiation patterns at (a)(b) 1.7 GHz, (c)(d) 2.7 GHz, (e)(f) 3.3 GHz and (g)(h) 3.6 GHz.

4. Conclusions

In this letter, a wideband dual-polarized dipole antenna operating at 1.7-3.8 GHz has been proposed. To restore the distorted antenna radiation patterns within 3.3-3.8 GHz, an AMC has been presented by developing a connected-ring-shaped metasurface or frequency selective surface structure.

This AMC structure was inserted between the antenna radiator and ground and therefore it did not increase the overall antenna height. The measured results revealed that the proposed antenna simultaneously obtained the wide impedance bandwidth of 76.4%, 7.0±1.0 stable realized gain, normal radiation patterns with 70±5° HPBW and simple structure. These merits make the proposed antenna a good candidate for the base station antenna applications.

Abbreviations

The following abbreviations are used in this manuscript:

AMC   Artificial Magnetic Conductor
HPBW   Half Power Beamwidth
CD   Crossed Dipole
BSA   Base Station Antenna

References

1. Ye, L.H.; Zhang, X.Y.; Gao, Y.; Xue, Q. Wideband Dual-Polarized Four-Folded-Dipole Antenna Array With Stable Radiation Pattern for Base-Station Applications. *IEEE Transactions on Antennas and Propagation* **2020**, *68*, 4428–4436. https://doi.org/10.1109/TAP.2020.2969749.
2. Wu, R.; Wen, G.H.; Liu, Y.; Chen, F.C. A Broadband Filtering Antenna Array for Sub-6 GHz Base Station Applications. *IEEE Antennas and Wireless Propagation Letters* **2024**, *23*, 394–398. https://doi.org/10.1109/LAWP.2023.3325621.
3. Wu, R.; Xue, Q.; Chu, Q.X.; Chen, F.C. Ultrawideband Dual-Polarized Antenna for LTE600/LTE700/GSM850/GSM900 Application. *IEEE Antennas and Wireless Propagation Letters* **2021**, *20*, 1135–1139. https://doi.org/10.1109/LAWP.2021.3073290.
4. Dai, X.; Luk, K.M. A Wideband Dual-Polarized Antenna for Millimeter-Wave Applications. *IEEE Transactions on Antennas and Propagation* **2021**, *69*, 2380–2385. https://doi.org/10.1109/TAP.2020.3043886.
5. Jiang, W.; Liao, S.; Che, W.; Xue, Q. Millimeter-Wave Wideband ±45° Dual-Polarized Phased Array Antenna Based on Compact Wideband Widebeam Dipole Element Antenna. *IEEE Antennas and Wireless Propagation Letters* **2023**, *22*, 1813–1817. https://doi.org/10.1109/LAWP.2023.3266063.
6. Li, B.; Yin, Y.Z.; Hu, W.; Ding, Y.; Zhao, Y. Wideband Dual-Polarized Patch Antenna With Low Cross Polarization and High Isolation. *IEEE Antennas and Wireless Propagation Letters* **2012**, *11*, 427–430. https://doi.org/10.1109/LAWP.2012.2195149.
7. Chu, Q.X.; Wen, D.L.; Luo, Y. A Broadband ±45° Dual-Polarized Antenna With Y-Shaped Feeding Lines. *IEEE Transactions on Antennas and Propagation* **2015**, *63*, 483–490. https://doi.org/10.1109/TAP.2014.2381238.
8. Huang, H.; Liu, Y.; Gong, S. A Broadband Dual-Polarized Base Station Antenna With Sturdy Construction. *IEEE Antennas and Wireless Propagation Letters* **2017**, *16*, 665–668. https://doi.org/10.1109/LAWP.2016.2598181.
9. Wen, L.H.; Gao, S.; Luo, Q.; Mao, C.X.; Hu, W.; Yin, Y.; Zhou, Y.; Wang, Q. Compact Dual-Polarized Shared-Dipole Antennas for Base Station Applications. *IEEE Transactions on Antennas and Propagation* **2018**, *66*, 6826–6834. https://doi.org/10.1109/TAP.2018.2871717.
10. Zhou, Z.; Wei, Z.; Tang, Z.; Yin, Y. Design and Analysis of a Wideband Multiple-Microstrip Dipole Antenna with High Isolation. *IEEE Antennas and Wireless Propagation Letters* **2019**, *18*, 722–726. https://doi.org/10.1109/LAWP.2019.2901838.

11. Li, Y.; Zhao, Z.; Tang, Z.; Yin, Y. Differentially-Fed, Wideband Dual-Polarized Filtering Antenna With Novel Feeding Structure for 5G Sub-6 GHz Base Station Applications. *IEEE Access* **2019**, *7*, 184718–184725. https://doi.org/10.1109/ACCESS.2019.2960885.

12. Ye, L.H.; Li, Y.J.; Wu, D.L. Dual-Wideband Dual-Polarized Dipole Antenna With T-Shaped Slots and Stable Radiation Pattern. *IEEE Antennas and Wireless Propagation Letters* **2022**, *21*, 610–614. https://doi.org/10.1109/LAWP.2021.3139454.

13. Fu, S.; Cao, Z.; Quan, X.; Xu, C. A Broadband Dual-Polarized Notched-Band Antenna for 2/3/4/5G Base Station. *IEEE Antennas and Wireless Propagation Letters* **2020**, *19*, 69–73. https://doi.org/10.1109/LAWP.2019.2953294.

14. Wen, L.H.; Gao, S.; Mao, C.X.; Luo, Q.; Hu, W.; Yin, Y.; Yang, X. A Wideband Dual-Polarized Antenna Using Shorted Dipoles. *IEEE Access* **2018**, *6*, 39725–39733. https://doi.org/10.1109/ACCESS.2018.2855425.

15. Zhao, L.; Zhu, H.; Zhao, H.; Liu, G.; Wang, K.; Mou, J.; Zhang, W.; Li, J. Design of Wideband Dual-Polarized ME Dipole Antenna With Parasitic Elements and Improved Feed Structure. *IEEE Antennas and Wireless Propagation Letters* **2023**, *22*, 174–178. https://doi.org/10.1109/LAWP.2022.3206331.

16. Ye, L.H.; Ye, D.G.; Chen, Z.; Li, J.F. Ultra-Wideband Dual-Polarized Base-Station Antenna With Stable Radiation Pattern. *IEEE Transactions on Antennas and Propagation* **2023**, *71*, 1919–1924. https://doi.org/10.1109/TAP.2022.3221024.

17. Peng, J.D.; Li, X.L.; Ye, L.H.; Li, J.F.; Wu, D.L.; Zhang, X.Y. Low-Profile Wideband Dual-Polarized Dipole Antenna With Parasitic Strips and Posts. *IEEE Antennas and Wireless Propagation Letters* **2023**, *22*, 844–848. https://doi.org/10.1109/LAWP.2022.3226506.

18. Yang, J.Y.; Ding, X.H.; Yang, W.W.; Chen, J.X. Compact Wideband Dual-Polarized Antenna Using Shared Dipoles Loaded With Partially Coupled Stubs. *IEEE Antennas and Wireless Propagation Letters* **2023**, *22*, 2886–2890. https://doi.org/10.1109/LAWP.2023.3303444.

19. de Cos, M.E.; Heras, F.L.; Franco, M. Design of Planar Artificial Magnetic Conductor Ground Plane Using Frequency-Selective Surfaces for Frequencies Below 1 GHz. *IEEE Antennas and Wireless Propagation Letters* **2009**, *8*, 951–954. https://doi.org/10.1109/LAWP.2009.2029133.